Strong Peak in T_c of Sr_2RuO_4 Under Uniaxial Pressure

Alexander Steppke,[1,2,*] Lishan Zhao,[1,2] Mark E. Barber,[1,2] Thomas Scaffidi,[3] Fabian Jerzembeck,[1] Helge Rosner,[1] Alexandra S. Gibbs,[2,4] Yoshiteru Maeno,[5] Steven H. Simon,[3,†] Andrew P. Mackenzie,[1,2,‡] and Clifford W. Hicks[1,§]

[1] *Max Planck Institute for Chemical Physics of Solids, Nöthnitzer Str. 40, 01187 Dresden, Germany*

[2] *Scottish Universities Physics Alliance (SUPA), School of Physics and Astronomy, University of St. Andrews, St. Andrews KY16 9SS, United Kingdom*

[3] *Rudolf Peierls Centre for Theoretical Physics, Oxford, 1 Keble Road, OX1 3NP, United Kingdom*

[4] *ISIS Facility, Rutherford Appleton Laboratory, Chilton, Didcot OX11 OQX, United Kingdom*

[5] *Department of Physics, Graduate School of Science, Kyoto University, Kyoto 606-8502, Japan*

(Dated: 21 Apr 2016)

We report a combined experimental and theoretical study of the dependence of the superconductivity of the unconventional superconductor Sr_2RuO_4 on anisotropic strain. Novel piezoelectric apparatus is used to apply uniaxial pressures of up to ∼1 GPa along a ⟨100⟩ direction (a-axis) of the crystal lattice. T_c increases from 1.5 K in unstrained material to 3.4 K at compression by ≈0.6%, then falls steeply. The c-axis upper critical field for the strained T_c = 3.4 K material is a factor of twenty larger than that of the unstrained crystal, whereas the in-plane (a-axis) critical field increases by only a factor of three. First-principles electronic structure calculations give evidence that the observed maximum T_c occurs at or near a Lifshitz transition when the Fermi level passes through a van Hove singularity. Finally, we perform order parameter analyses using three-band renormalization group calculations. These, combined with the unexpectedly low in-plane critical field, open the possibility that the highly strained T_c=3.4 K Sr_2RuO_4 has an even- rather than an odd-parity order parameter. Potential implications such as a transition at nonzero strain between odd- and even-parity order parameters are discussed.

Introduction

The formation of superconductivity by the condensation of electron pairs into a coherent state is one of the most spectacular many-body phenomena observed in physics. For nearly seventy years after its discovery, all known superconducting condensates were of the same basic class, in which electrons paired into spin-singlet states, forming condensates of even parity whose phase ϕ is independent of wave vector $\mathbf{k}$ [1]. Condensates of this form have the useful property of being insensitive to the presence of non-magnetic scattering, and so are easier to observe in materials grown with standard levels of disorder. In the last three decades, a richer and more exciting picture has emerged. In the growing number of known unconventional superconductors, the condensate order parameters have strong $\mathbf{k}$ dependence of both ϕ and the energy gap $|\Delta|$, can have both even and odd parity, and are sensitive to the presence of disorder [2, 3]. These new materials give a unique opportunity to study the collective physics of interacting electrons and the mechanisms by which the condensation from the normal metallic state occurs. However, in order to access the new physics to its fullest extent, considerable material and experimental challenges must be overcome.

The subject of the research described in this paper, Sr_2RuO_4 (transition temperature $T_c \approx 1.5$ K) [4], is the most disorder-sensitive of all known superconductors [5]. However the stringent requirements this places on material purity also bring advantages. The long mean free paths of ∼1 μm that are required to observe its superconductivity in the clean limit have also enabled extensive studies of its normal state via the de Haas-van Alphen effect [6]. This work, combined with angle-resolved photoemission experiments [7] and electronic structure calculations [8–10], has led to a detailed understanding of the quasi-2D Fermi surface topography and the effective masses of the Landau Fermi liquid quasiparticles which pair to form the superconducting condensate.

This depth of understanding of the normal state of Sr_2RuO_4, combined with its relative simplicity, gives the hope

that a full understanding of the superconductivity can be achieved. However, in spite of over two decades of work, the order parameter is not known with certainty. Soon after the discovery of the superconductivity, the similarity of the Landau parameters of Sr_2RuO_4 to those of the famous p-wave superfluid ^{3}He led to the proposal that it might be an odd-parity superconductor with spin-triplet p-wave pairing [11]. Knight shift measurements [12, 13] and, recently, proximity-induced superconductivity in epitaxial ferromagnetic $SrRuO_3$ layers [14] provide strong evidence for triplet pairing. Muon spin rotation [15] and Kerr rotation [16] experiments point to time reversal symmetry breaking at T_c, and tunneling spectroscopy to chiral edge states [17]. Josephson interferometry indicates the presence of domains in the superconducting state and gives evidence for odd parity [18, 19]. In combination, these observations suggest the existence of a chiral, spin-triplet superconducting state with an order parameter of the form $p_x \pm ip_y$. Although the edge currents predicted for chiral p-wave order are not seen [20–22], there are proposals to explain why these might be unobservably small in Sr_2RuO_4 [23–26]. More difficult to understand for spin triplet pairing is why the upper critical field H_{c2} for in-plane fields is first-order at low temperatures [27] and smaller than predictions for orbital limiting based on anisotropic Ginzburg-Landau theory [28]. More complete reviews of the superconductivity of Sr_2RuO_4 and arguments for and against various order parameters can be found in Refs. [29–32].

The electronic structure of Sr_2RuO_4 is relatively simple compared with that of many unconventional superconductors. Its Fermi surfaces are known with accuracy and precision [6] and it shows good Fermi liquid behavior in the normal state [33]. Therefore, gaining a full understanding of the superconductivity of Sr_2RuO_4 is an important challenge and a benchmark for the field. An approach not extensively explored so far is to perturb the underlying electronic structure as far as possible from its native state and observe the effects on the superconductivity. Partial substitution of La for Sr [34] and epitaxial thin film growth on lattice-mismatched substrates [35] have both been used to push one of the Fermi surface sheets of Sr_2RuO_4 through a Lifshitz transition, *i.e.* a topological change in the Fermi surface, and an associated van Hove singularity (vHS) in the density of states. This is a major qualitative change in the electronic structure, and it would be interesting to see how the superconductivity responds. However, the disorder sensitivity of the superconductivity of Sr_2RuO_4 is so strong that it was not possible to do either experiment in a sufficiently clean way for any superconductivity to survive.

In principle, uniaxial pressure has the potential for tuning the electronic structure of Sr_2RuO_4 without introducing disorder and destroying the superconductivity. Pressure applied along a $\langle 100 \rangle$ lattice direction, lifting the native tetragonal symmetry of Sr_2RuO_4, has been shown to increase the bulk T_c to at least 1.9 K [36]. There are hints that $T_c \sim 3$ K in pure Sr_2RuO_4 is achievable with lattice distortion [37, 38], however it has only been seen locally, which complicates determination of its origin and properties. By extending the piezoelectric-based compression techniques introduced in Ref. [36] to achieve much higher compressions, we demonstrate in this work the existence of a well-defined peak in T_c at 3.4 K, at approximately 0.6% compression. The Young's modulus of Sr_2RuO_4 is 176 GPa [39], so this compression corresponds to a uniaxial pressure of $\sim$1 GPa. The factor of 2.3 increase in T_c is accompanied by more than a factor of twenty enhancement of H_{c2} for fields along the c-axis. We complement our experimental observations with two classes of calculation. Density functional theory (DFT) calculations give evidence that the peak in T_c likely coincides with a Lifshitz transition. Then, to gain insight into the effect of these large strains on possible superconducting order parameters of Sr_2RuO_4, we employ weak-coupling renormalization group (RG) calculations that include spin-orbit and interband couplings, extending the work of Ref. [40].

Results

For guidance on the likely effect of strain on the electronic structure, we start with the results of the DFT calculations of the band structure of Sr_2RuO_4. Unstrained lattice parameters were taken from the $T = 15$ K data of Ref. [41]. In the experiment, the sample is a high-aspect-ratio bar that is compressed or tensioned along its length, so in the calculation the longitudinal strain ε_{xx} is an independent variable, and the transverse strains are set, as in the experiment, according to the Poisson's ratios of Sr_2RuO_4: $\varepsilon_{yy} = -\nu_{xy}\varepsilon_{xx}$, and $\varepsilon_{zz} = -\nu_{xz}\varepsilon_{xx}$ [39]. The robustness of the results against different approximations was verified by calculations with a moderate density of k-points; more details are given in Supplemental Material. The final calculations, made in the local density approximation with spin-orbit coupling and apical oxygen position relaxation, were then extended to 343,000 k-points: due to proximity of the vHS to the Fermi level, an unusually large number of k-points was required for convergence. The first Lifshitz transition was found to occur with a compressive strain of $\varepsilon_{xx} = \varepsilon_{\mathrm{vHS}} \approx -0.0075$. The calculated Fermi surfaces at $\varepsilon_{xx} = 0$ and $\varepsilon_{xx} = \varepsilon_{\mathrm{vHS}}$ are shown in Fig. 1, where it can be seen that compression along $\hat{\mathbf{x}}$ leads to a Lifshitz

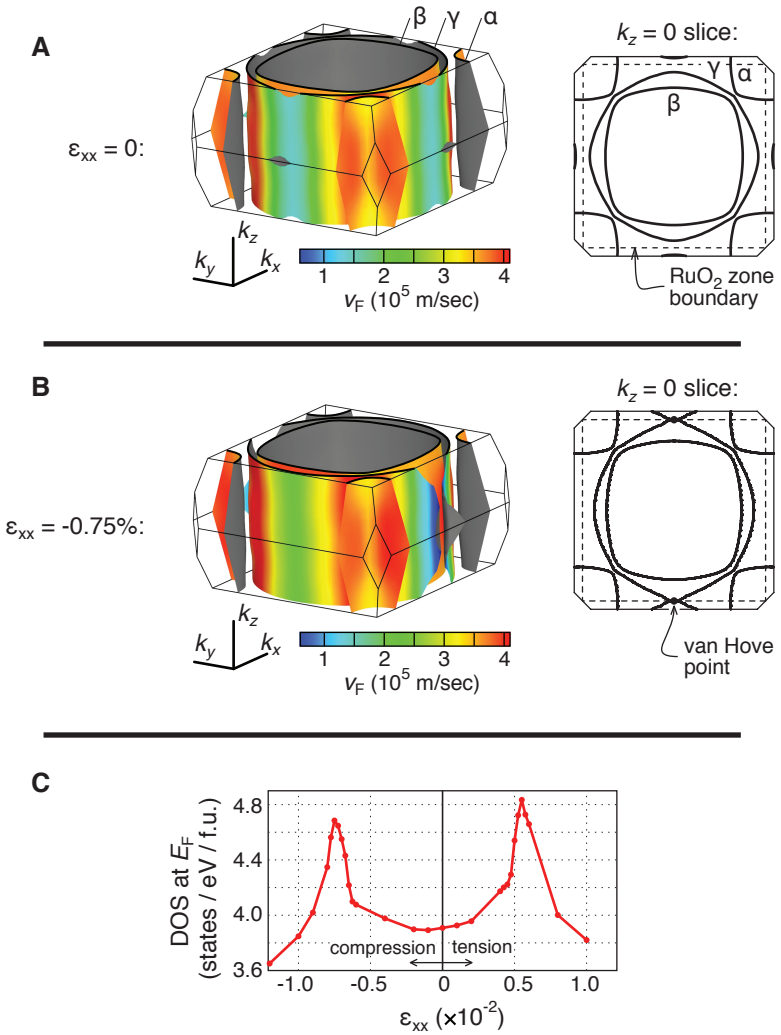

FIG. 1: **DFT calculation results. A.** Calculated Fermi surfaces of unstrained Sr_2RuO_4, colored by the Fermi velocity v_F, at zero strain. The three surfaces are labeled α, β, and γ. A cross-section through $k_z = 0$ is also shown. The dashed lines indicate the zone of an isolated RuO_2 sheet; in 2D models of Sr_2RuO_4, the van Hove point is located on this zone boundary. **B.** Calculated Fermi surfaces at $\varepsilon_{xx} = -0.0075$. **C.** Calculated total density of states against ε_{xx}.

transition in the γ Fermi surface along k_y. Due to the low k_z dispersion, it occurs for all k_z over a very narrow range of ε_{xx}, starting at $\varepsilon_{xx} = (-0.75 \pm 0.01) \times 10^{-2}$ and finishing by $(-0.77 \pm 0.01) \times 10^{-2}$. Cross-sections at $k_z = 0$ are also shown. In fully 2D approximations of Sr_2RuO_4 the Lifshitz transition occurs at a single van Hove point, that is labeled in the figure and coincides with the 2D zone boundary of an isolated RuO_2 sheet. (The 3D case is slightly more complicated and discussed in Supplemental Material.) Shown in panel C is the calculated change in the total density of states (DOS) as a function of tensile and compressive strains. The sharp maxima indicate Lifshitz transitions, and should be taken as only a qualitative guide to expectations for real Sr_2RuO_4, in which many-body effects are likely to strengthen the quasiparticle renormalization of v_F and the DOS in the vicinity of the peaks. The peak on the tension side corresponds to a Lifshitz transition along k_x, which is not accessible experimentally because samples break under strong tension.

We now describe the experiment. The apparatus is based on that presented in Refs. [36] and [42], but modified to achieve the larger strains required for the current project. Samples were cut with a wire saw into high-aspect-ratio bars and annealed at 450° C for two days in air, to partially relax dislocations created by the cutting. Their ends were secured in the apparatus with epoxy [43] as illustrated in Fig. 2. Piezoelectric actuators push or pull on one end to strain the exposed central portion of the sample; to achieve high strains, 18 mm-long actuators are used, instead of the 4 mm-long ones used previously. Because samples break under strong tension, here we worked almost exclusively

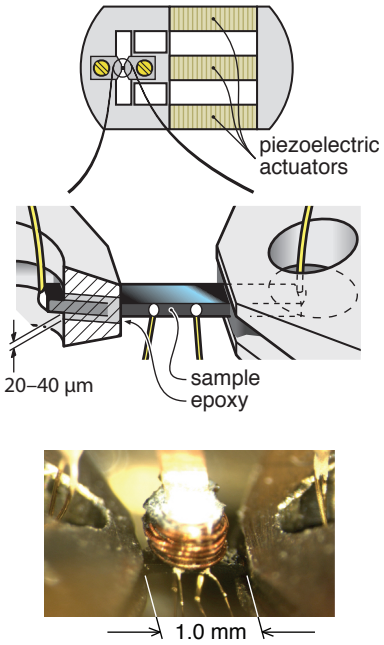

FIG. 2: **Apparatus and sample configuration.** Top: apparatus configuration. Extending the outer two piezoelectric actuators tensions the sample, and extending the central actuator compresses the sample. Middle: sample configuration. The ends are secured with epoxy. Some samples have contacts for resistivity measurements, which are also shown in the schematic. Bottom: a photograph of sample 3. On top of the sample, mounted on a flexible cantilever, are concentric coils used for measuring magnetic susceptibility.

with compression. The superconducting transitions were measured magnetically, by measuring the mutual inductance between two coils of diameter $\lesssim 1$ mm placed near the centre of the sample. The r.m.s. excitation field applied was $\sim$ 0.2 Oe, mostly parallel to the samples' c axes. Some samples also had electrical contacts for resistivity measurements.

Five samples were measured in total, and all gave consistent results. Fig. 3 shows the real part of the magnetic susceptibility χ' against temperature at various compressive strains for two samples, with zero-strain T_c's of 1.43 and 1.26 K. The strains are determined using a parallel-plate capacitive displacement sensor incorporated into the apparatus. We estimate $\sim 20\%$ uncertainty in the strain determination, originating primarily in uncertainty on how the epoxy securing the sample deforms as force is applied. When the sample is initially compressed, the transition moves to higher temperature, and broadens somewhat. This broadening differs in form and magnitude from sample to sample, so is probably extrinsic. For example, imperfection in the sample mounts is likely to lead to some sample bending as force is applied, imposing a strain gradient across the thickness of the sample, and in addition a low density of dislocations and/or ruthenium inclusions may introduce some internal strain disorder. However, in spite of the likely presence of some strain inhomogeneity, the transition becomes very sharp as it approaches the maximum T_c, 3.4 K for the first and 3.2 K for the second sample. The second sample could be compressed well beyond this maximum, and T_c was found to drop rapidly. In checks made on multiple samples the response was found to be fully elastic: on releasing the strain and returning to $\varepsilon_{xx} \sim 0$, the $\chi'(T)$ curves were found to be unchanged.

The peak in T_c can be clearly seen in the graph of T_c against ε_{xx} for three samples, including these two, shown in Fig. 4. The strain scales have been normalized in the plot. ε_{xx} at the peak, from averaging independent determinations from four samples, is $(-0.60 \pm 0.06) \times 10^{-2}$. The plot is based exclusively on magnetic measurements. On samples where the resistivity was measured, the resistive T_c's never exceeded the highest magnetic T_c by more than 0.08 K, confirming that it is the maximum T_c.

The apparatus is constructed of nonmagnetic materials, allowing measurement of the superconducting critical fields. A further sample was mounted in a vector magnet, with the pressure axis (a $\langle 100 \rangle$ lattice direction) parallel to the magnet z-axis, allowing the c-axis and in-plane upper critical fields to be measured in a single cool-down. The very sharp transitions in $\chi'(T)$ of Sr_2RuO_4 compressed to the peak in T_c (referred to henceforth as $T_c = 3.4$ K Sr_2RuO_4) make determination of T_c and H_{c2} very simple: in all temperature and field ramps a sharp cusp in $\chi'(T)$ was observed,

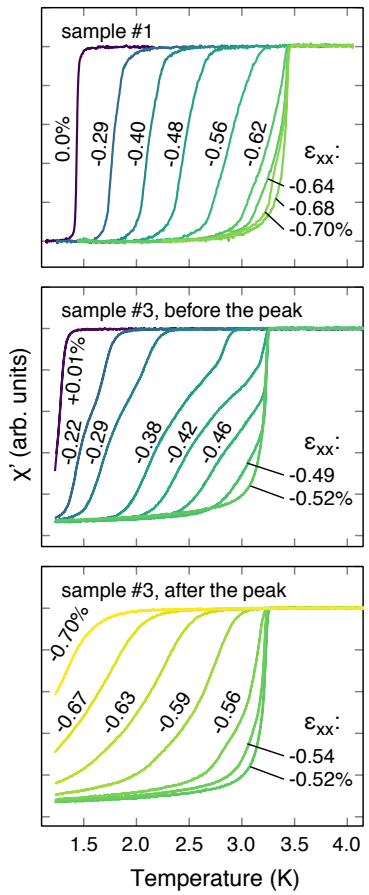

FIG. 3: **Susceptibility against temperature.** Top: real part of the susceptibility χ against temperature for sample 1, at various ε_{xx}. No normalizations or offsets are applied to the curves. Middle and bottom: same, for sample 3.

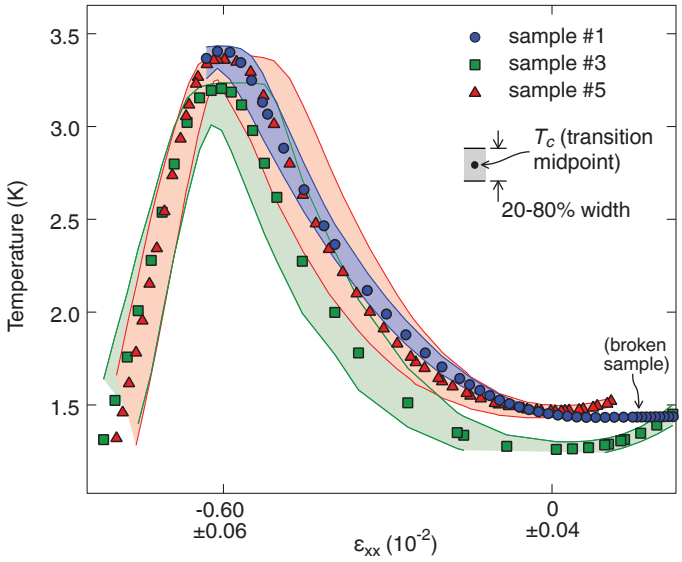

FIG. 4: T_c **against strain for three samples.** The points are the midpoints (50% levels) of the transitions shown in Fig. 3, and the lines are the 20 and 80% levels, giving a measure of the transition width. The strain scales have been normalized; the strain at the peak, $(-0.60 \pm 0.06) \times 10^{-2}$, is an average from independent determinations on four samples. The flat region around $\varepsilon_{xx} = 0$ for sample 1 is an artefact: the sample broke during cool-down, meaning that tensile strain could not be applied, and that a compressive strain was required for it to re-engage.

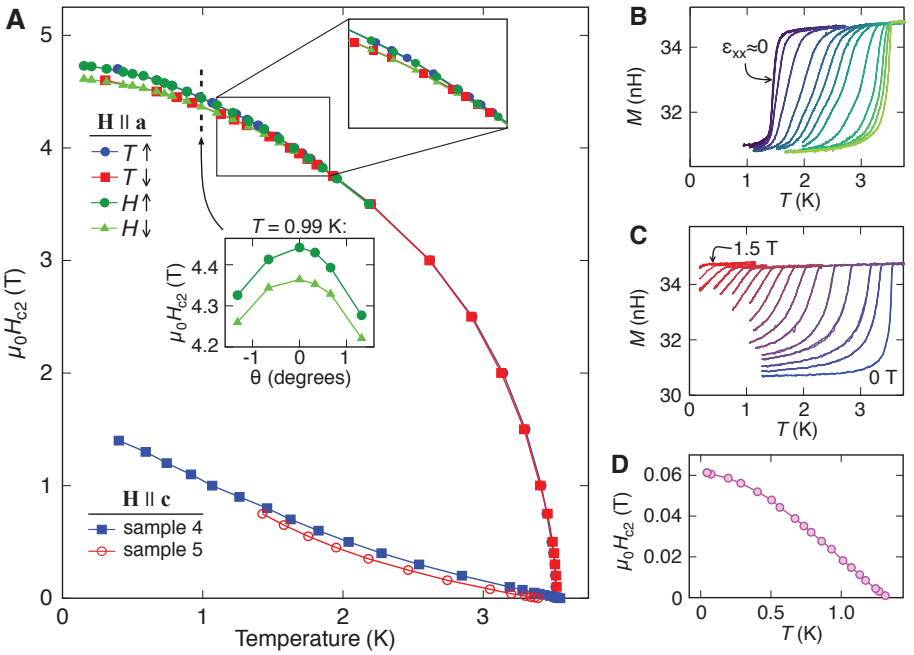

FIG. 5: H_{c2} **against temperature. A.** $H_{c2\|a}$ and $H_{c2\|c}$ against temperature for sample 4, compressed to the peak in T_c. $H_{c2\|a}$ measured with both field and temperature ramps, and found to be hysteretic below ∼1.8 K. An inset shows the angle dependence of H_{c2} at 990 mK, to confirm the field alignment. θ is the angle in the **a-c** plane, and $\theta = 0$ the field angle at which the $H_{c2\|a}$ data were collected. **B.** Raw data for $\chi'(T)$ of sample 4 at various ε_{xx}. The y scale is the mutual inductance of the measurement coils. **C.** Measured $\chi'(T)$ at the peak in T_c, and at fields in 0.1 T increments between 0 and 1.5 T. **D.** Data for $H_{c2\|c}$ of unstrained Sr_2RuO_4, from Ref. [46].

which could be identified as T_c or H_{c2}. Specifically, the transition was identified as the intersection of linear fits to data just below and above the cusp. The in-plane H_{c2} of Sr_2RuO_4 is known to be very sensitive to precise alignment of the field with the plane, so the vector field capability was used to align the field to within 0.2° of the ab plane. Within the ab plane, the alignment to the $\langle 100 \rangle$ direction is with standard ∼3° precision. In long field ramps the magnet was found to have ∼0.1 T-scale hysteresis, so when field ramps were performed the transition was first located approximately, and then precisely with up- and down-ramps over a 0.35 T range, for which the magnet hysteresis was found to be ∼10 mT.

Results are shown in Fig. 5. The c-axis H_{c2}, $H_{c2\|c}$, of $T_c = 3.4$ K Sr_2RuO_4 is concave, and at $T \to 0$ slightly exceeds the limit of the in-plane coils of the vector magnet, 1.5 T. For in-plane fields, the upper critical field $H_{c2\|a}$ reaches 4.7 T as $T \to 0$, and both temperature and field ramps show that the transition is first-order below $\approx$ 1.8 K.

A concave $H_{c2}(T)$ curve is an indication of high gap non-uniformity, *i.e.* substantially different gap magnitudes on different Fermi sheets, or strong variation within each sheet, or both. It has been seen in *e.g.* MgB_2 [44] and $Be(Fe,Co)_2As_2$ [45]. In $T_c = 3.4$ K Sr_2RuO_4, the slope $|dH_{c2\|c}/dT|$ is found to steadily increase to the lowest temperatures measured, although $H_{c2\|c}(T)$ must eventually become convex because dH_{c2}/dT must approach zero as $T \to 0$. Also shown in the figure is $H_{c2\|c}$ of unstrained Sr_2RuO_4, from Ref. [46]. It is weakly concave at higher temperatures, but only above $\sim$ 0.7 K, a much higher fraction of $T_c(H = 0)$ than the concave-convex crossover in $T_c = 3.4$ K Sr_2RuO_4. This difference in the $H_{c2}(T)$ curves indicates that the gap varies more widely across the Fermi surfaces in $T_c = 3.4$ K Sr_2RuO_4 than in unstrained Sr_2RuO_4.

The $T \to 0$ critical field values for $T_c = 3.4$ K Sr_2RuO_4 are striking. $H_{c2\|c}(T \to 0)$ is enhanced by more than a factor of twenty relative to unstrained Sr_2RuO_4, while $H_{c2\|a}(T \to 0)$ is enhanced by a factor of only ≈ 3. In the simplest picture of a fully two-dimensional triplet superconductor with the spins in the plane, the ratio γ_s between $H_{c2\|a}$ and $H_{c2\|c}$ would be infinite, because neither orbital nor Pauli limiting would apply for in-plane fields. However we observe that γ_s is reduced from a value of $\approx$ 20 in unstrained Sr_2RuO_4 to $\approx$ 3 in $T_c = 3.4$ K Sr_2RuO_4. The

electronic structure calculations presented in Fig. 1 indicate that Sr_2RuO_4 remains quasi-2D at high strains, a result supported by the observation in Fig. 5 that just below T_c the slope $|dH_{c2\|a}/dT|$ far exceeds $|dH_{c2\|c}/dT|$. Therefore it seems unlikely that an orbital limiting effect could cause such a reduction in γ_s. In contrast, the first-order nature of the transition under strong in-plane field is consistent with a hypothesis of Pauli limiting [47], as is the absolute value of $H_{c2\|a}$. In a mean-field superconductor both T_c and the Pauli-limited H_{c2} are expected to vary linearly with the $T \to 0$ gap magnitude $|\Delta|$ [48]. $H_{c2\|a}$ of unstrained Sr_2RuO_4 is 1.5 T, so the rise to 4.7 T in $T_c = 3.4$ K Sr_2RuO_4 is somewhat but not drastically faster than linear against T_c. In combination, these observations motivate investigation of whether the $T_c = 3.4$ K state might be an even-parity condensate of spin-singlet pairs.

In fact, a qualitative analysis of the enhancement of $H_{c2\|c}$ also points to this possibility. In a mean-field superconductor, the orbitally-limited $H_{c2}(T \to 0)$ is proportional to a weighted average of $[|\Delta|N(E_F)]^2$, where $N(E_F)$ is the Fermi surface density of states. Since T_c is proportional to a k-space average of $|\Delta|$, if $|\Delta(\mathbf{k})|$ is multiplied by a factor and $N(E_F)$ is not modified, the quantity H_{c2}/T_c^2 should remain constant. In strained Sr_2RuO_4, $N(E_F)$ increases strongly near the van Hove point, so a strong increase in H_{c2}/T_c^2 likely requires large $|\Delta|$ in this region of the Brillouin zone. However, the van Hove point is invariant under inversion, so $|\Delta|$ of an odd parity order parameter must be zero at the van Hove point and parametrically small in its vicinity. Qualitatively, one might therefore expect stronger enhancement of H_{c2}/T_c^2 for even-parity order, for which large $|\Delta|$ is allowed near the van Hove points, than for odd-parity order, where $|\Delta|$ must be small in just the regions where $N(E_F)$ is largest. Our observation that $H_{c2\|c}/T_c^2$ is enhanced by a factor of four in $T_c = 3.4$ K Sr_2RuO_4 provides qualitative evidence that the order parameter of $T_c = 3.4$ K Sr_2RuO_4 is even- rather than odd-parity.

To investigate these qualitative arguments in more depth and on the basis of a realistic calculation taking into account the multi-sheet Fermi surface of Sr_2RuO_4, we have extended a 2D weak-coupling renormalization group calculation, presented by some of the authors in Ref. [40] as an extension of ideas first presented in Ref. [49], to strained Sr_2RuO_4. The weak-coupling approximation allows an unbiased comparison of different possible superconducting order parameters. In this calculation, a tight-binding model of all three Fermi surfaces of Sr_2RuO_4 is specified (and given in Supplemental Material), including the effects of spin-orbit and interband coupling. The remaining free parameter is the ratio of Hund's coupling to Hubbard interaction, J/U. In Ref. [40], it was found that two ranges of J/U give gap anisotropy consistent with specific heat data [50]: $J/U \sim 0.08$ and $J/U \sim 0.06$. Both yield odd-parity pairing; the higher range gives helical order ($\mathbf{d} \sim p_x\hat{\mathbf{x}} + p_y\hat{\mathbf{y}}$) with $|\mathbf{d}|$ slightly larger on the α and β sheets, while the lower value favours chiral order [$\mathbf{d} \sim (p_x \pm ip_y)\hat{\mathbf{z}}$] and $|\mathbf{d}|$ slightly larger on γ. $\mathbf{d}$ is the so-called d-vector, that describes a spin-triplet order parameter, including its spin structure. For states of the type considered here, the energy gap $|\Delta|$ equals $|\mathbf{d}|$.

Here, we present $J/U = 0.06$ results for strained Sr_2RuO_4; the $J/U = 0.08$ results are similar and are shown in Supplemental Material. At zero strain, the point group symmetry of the lattice is D_{4h}, and $(p_x \pm ip_y)\hat{\mathbf{z}}$ and $d_{x^2-y^2}$ are respectively the most favoured odd- and even-parity irreducible representations. At nonzero strain, the point group symmetry becomes D_{2h}. $(p_x \pm ip_y)\hat{\mathbf{z}}$ is resolved into the separate irreducible representations $p_x\hat{\mathbf{z}}$ and $p_y\hat{\mathbf{z}}$, and $d_{x^2-y^2}$ becomes $d_{x^2-y^2} + s$. Strain is simulated by introducing anisotropy into the hopping integrals. The nearest-neighbor hopping t, for example, is resolved into $t_x = t \times (1 + a\varepsilon_{xx})$ and $t_y = t \times (1 - a\nu_{xy}\varepsilon_{xx})$, where a is chosen such that the Lifshitz transition occurs at $\varepsilon_{xx} = -0.0075$, in agreement with the LDA+SOC calculation.

$p_y\hat{\mathbf{z}}$ and $p_x\hat{\mathbf{z}}$ are respectively the highest-T_c order parameters under compression and tension; compression favors p_y because it increases the DOS on the sections of Fermi surface where p_y order has the largest gap magnitude, and similarly for tension and p_x. For $J/U = 0.06$ the possible helical orders ($\mathbf{d} \sim p_x\hat{\mathbf{x}} \pm p_y\hat{\mathbf{y}}$ or $p_x\hat{\mathbf{y}} \pm p_y\hat{\mathbf{x}}$) have lower T_c at all strains calculated. Results for T_c against ε_{xx} for $p_x\hat{\mathbf{z}}$, $p_y\hat{\mathbf{z}}$, and $d_{x^2-y^2} + s$ orders are shown in Fig. 6. T_c of the p_x and p_y orders cross at $\varepsilon_{xx} = 0$, as they must [51], and the slope $|dT_c/d\varepsilon_{xx}|$ as $\varepsilon_{xx} \to 0$ is ∼0.3 K/%. This crossing would appear as a cusp in a $T_c(\varepsilon_{xx})$ curve derived from measurements that detect only the higher T_c, and to search for this cusp was the primary aim of Ref. [36]. Although no cusp was seen, the resolution of the experiment does not rule out a cusp of this magnitude, and it could also be rounded by fluctuations [52]. At higher strains, T_c of both even- and odd-parity orders is found to peak at $\varepsilon_{xx} \approx \varepsilon_{\mathrm{vHS}}$. (The equivalent peaks on the tension side, as noted above, are not accessible experimentally.) Odd-parity order is found to be favoured at nearly all strains, however T_c of the even-parity order is found to peak more strongly as the van Hove singularity is approached; in the immediate vicinity of the vHS, even- and odd-parity orders are nearly degenerate.

The k-space structure of the favored odd- and even-parity orders at $\varepsilon_{xx} = 0$ and $\varepsilon_{\mathrm{vHS}}$ is shown in Fig. 7. For both

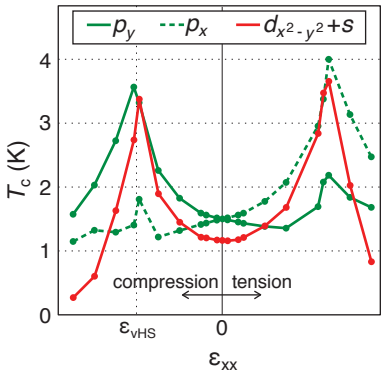

FIG. 6: **Weak-coupling RG results: T_c versus strain.** The bandwidth and U/t were set to reproduce the experimental values of $T_c(0) = 1.5$ K, and $T_c(\varepsilon_{\rm vHS}) \sim 3.4$ K. $p_x \pm ip_y$ and $d_{x^2-y^2}$ are irreducible representations of the $\varepsilon_{xx} = 0$ (*i.e.* tetragonal) lattice. For $\varepsilon_{xx} \neq 0$, $p_x \pm ip_y$ is resolved into separate representations p_x and p_y, and $d_{x^2-y^2}$ becomes $d_{x^2-y^2} + s$.

parities, the structure of $\Delta(\mathbf{k})$ is quite complicated; $p_x \pm ip_y$, p_y, etc. are labels of the irreducible representation, not accurate descriptions of the full gap structure. At $\varepsilon_{xx} = \varepsilon_{\rm vHS}$ the p_y order has two nodes on the γ sheet: one at $(0, \pi)$, where the γ sheet touches the zone boundary and odd-parity orders must have zero amplitude, and the other along $(k_x, 0)$, where p_y order has zero amplitude by symmetry. Also, whereas at zero strain the odd-parity $|\Delta|$ is generally largest on the γ sheet, at $\varepsilon_{xx} = \varepsilon_{\rm vHS}$ it is larger on the α and β sheets, due to the frustration for odd-parity order at the van Hove point on the γ sheet. T_c still peaks at $\varepsilon_{\rm vHS}$ because the small-$\mathbf{q}$ fluctuations on γ, that diverge at $\varepsilon_{\rm vHS}$, also contribute to superconductivity on α and β through inter-orbital interaction terms. In contrast, even-parity order does not suffer frustration at the van Hove point, so its gap remains largest on γ, and its T_c peaks more strongly at $\varepsilon_{\rm vHS}$.

Following Ref. [53], we calculate the orbital-limited $H_{c2\|c}/T_c^2$ at various applied strains in the semi-classical approximation. The full expression is given in Supplemental Material; an abbreviated form is: $H_{c2} \propto T_c^2 \exp(-2\langle|\psi_\mu|^2 \log \tilde{v}_\mu\rangle)$. $\langle ...\rangle$ is a Fermi surface average, $\psi(\mathbf{k}) \propto \Delta(\mathbf{k})$, μ is a band index, and $\tilde{v}$ is a velocity derived from the Fermi velocity. The results support the qualitative arguments made above and are shown in Fig. 8. For odd-parity order the shift of the gap onto these sheets causes a decrease in $H_{c2\|c}/T_c^2$, because the α and β sheets have lower DOS than the γ sheet. In contrast, the increased DOS around the van Hove point causes $H_{c2\|c}/T_c^2$ of $d_{x^2-y^2} + s$ order to increase towards the vHS. The actual $H_{c2\|c}/T_c^2$ may be enhanced over the weak-coupling results by strengthened many-body effects towards the vHS, however the results emphasize a strong quantitative disparity between $H_{c2\|c}/T_c^2$ for even- and odd-parity order parameters.

Discussion

One long-standing puzzle in the physics of Sr_2RuO_4 has been the origin of the so-called 3 K phase, which is $T_c \sim 3$ K superconductivity observed in eutectic crystals containing inclusions of Ru metal in a matrix of Sr_2RuO_4 [54]. It has been established that this higher-T_c superconductivity has a low volume fraction [54, 55], showing that it occurs at the inclusions rather than the bulk, and further that it occurs on the Sr_2RuO_4 side of Ru-Sr_2RuO_4 interfaces [56]. It now seems very likely that internal strain is the origin of the 3 K phase, although full proof would require observation of the strain fields around Ru inclusions. The upper critical fields of the 3 K phase have been obtained through measurement of resistivity along extended inclusions, and were found to be ∼1 T for c-axis and ∼3.5 T for in-plane fields [57]. The similarity of these fields with the critical fields of bulk $T_c = 3.4$ K Sr_2RuO_4 further supports the hypothesis that the 3 K phase is a local strain effect, although it is also possible that the observed 3 K phase critical fields are enhanced by the two-dimensional geometry of interface superconductivity [57, 58].

Three-band models in Refs. [59] and [60], in addition to the RG calculations presented here, identify the proximity of the γ sheet to a vHS as an important factor in the superconductivity of Sr_2RuO_4. Simultaneous to this work, calculations in Refs. [61] and [62] have found increasing T_c, at least initially, on tuning towards the vHS with strain. Our data do not prove, however, that the 3.4 K peak in T_c in fact coincides with the Lifshitz transition. That it

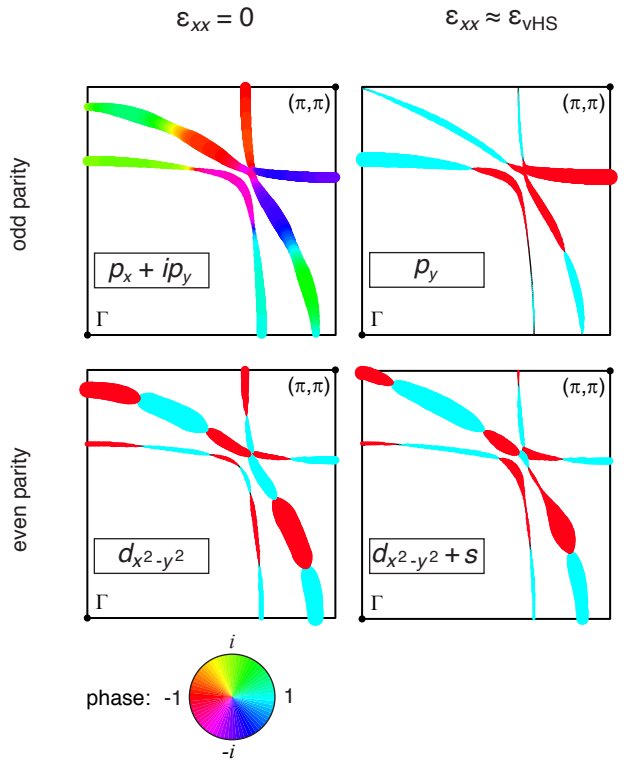

FIG. 7: **Weak-coupling RG results: order parameters.** Top: The odd-parity order parameter at $\varepsilon = 0$ and $\varepsilon \approx \varepsilon_{\rm vHS}$; the vHS is reached at $(0, \pi)$. The width of the traces is proportional to the energy gap, and the color indicates the phase. For $\varepsilon_{xx} \neq 0$, $p_x \pm ip_y$ is no longer an irreducible representation of the lattice, so the p_y representation, the favoured order parameter for $\varepsilon_{xx} < 0$, is shown instead. Bottom: even-parity order, at $\varepsilon = 0$ and $\varepsilon \approx \varepsilon_{\rm vHS}$.

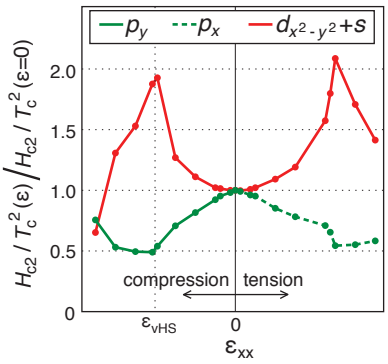

FIG. 8: **Weak-coupling RG results:** $H_{c2\|c}/T_c^2$ **versus strain.** The results are normalized to the $H_{c2\|c}/T_c^2$ calculated at zero strain.

occurs at a similar strain to $\varepsilon_{\rm vHS}$ determined from DFT calculations is suggestive that it does, but this is not strong evidence. Another possibility is that T_c of an odd-parity order initially increases, due to the increase in DOS induced by compression, but then decreases as frustration at the van Hove point becomes important. This is not the behavior indicated by the RG calculations, where T_c of p_y order peaks at $\varepsilon_{\rm vHS}$, but may still be considered a qualitative possibility. A further possibility, from Ref. [62], is that compression stabilizes competing spin density wave order that cuts off the superconductivity. Both mechanisms would cause the peak in T_c to precede the Lifshitz transition.

Other experimental tests are required to probe whether the T_c peak and Lifshitz transition coincide. However, this issue is not of great importance to the main conclusions that we draw here, because the substance of the comparison of the critical fields of $T_c = 3.4$ K and unstrained Sr_2RuO_4 stands regardless. The weak-coupling RG calculations yield strongly divergent trends for $H_{c2\|c}/T_c^2$ for even- and odd-parity order at all intermediate strains, not only at

the vHS, and because this is a result of frustration of odd-parity order in the vicinity of the van Hove point it is unlikely to be strongly model-dependent. Also, the arguments for Pauli limiting of $H_{c2\|a}(T \to 0)$ are unaffected by whether the peak is at the Lifshitz transition. The critical field comparisons clearly raise the possibility that the $T_c = 3.4$ K superconductivity has an even-parity, spin-singlet order parameter. It is difficult to understand in a naive analysis how the critical field anisotropy γ_s could be only ≈ 3 without Pauli limiting of $H_{c2\|a}$. However most current theories of Sr_2RuO_4 are two-dimensional and make no predictions for γ_s; we believe our observations provide strong motivation for extending realistic three-band calculations into the third dimension.

If the 3.4 K superconducting state is even-parity, there are two obvious possibilities, both exciting, for its relationship with the superconductivity of unstrained Sr_2RuO_4. One is that the evolution of the order parameter is continuous between the two states, and unstrained Sr_2RuO_4 is also an even-parity superconductor. However in this case a substantial body of experimental evidence [30] for triplet, chiral order would require alternative explanation. The evidence for chirality could be accommodated by a spin-singlet state, $d_{xz} \pm id_{yz}$ [63], however this state has horizontal line nodes and requires interplane pairing, which would be surprising in such a highly two-dimensional material. The other possibility is that there is a transition at an intermediate strain between odd- and even-parity states. At such a transition a kink, possibly weak, is expected in $T_c(\varepsilon_{xx})$, and a more prominent jump in $H_{c2\|c}(T \to 0)$. An important follow-up experiment therefore is measurement of $H_{c2\|c}$ at intermediate strains. This has not been done yet because the broadening of the transitions at intermediate strains complicates accurate determination of H_{c2}, and higher-precision sample mounting methods may be required.

Consideration of an odd-to-even-parity transition at intermediate strains is also motivated by evidence for interference between the superconductivity of Ru inclusions and that of bulk Sr_2RuO_4, and for hysteresis and switching behavior in Ru/Sr_2RuO_4 systems. The possible interference appears as a sharp drop in the critical current I_c of $Pb/Ru/Sr_2RuO_4$ junctions at T_c of Sr_2RuO_4 [64, 65], which has been interpreted as an onset of phase frustration at the Ru/SRO interface. However it could perhaps also be explained by appearance of an odd-parity/even-parity interface around the Ru inclusion. Similarly, hysteretic I_c has been seen in $Sr_2RuO_4/Cu/Pb$ [18], $Nb/Ru/Sr_2RuO_4$ [66], and $Pb/Ru/Sr_2RuO_4$ [65] junctions, and microbridges of Sr_2RuO_4 with Ru inclusions [67]. The former two also showed time-dependent switching noise. All these results have been interpreted as motion of $p_x + ip_y/p_x - ip_y$ domain walls, however even/odd domain walls appear to be a viable alternative possibility.

Our observations also give cause for optimism concerning the prospects of finding superconductivity in biaxially strained thin films: the factor-of-twenty $H_{c2\|c}$ enhancement corresponds to a factor of 4.5 reduction in the coherence length, considerably reducing the disorder constraint. Evidence for this is seen in Fig. 4: the T_c of the slightly disordered sample 3 is 0.17 K lower than that of sample 1 at zero strain, and 0.20 K lower at the peak T_c. This change is consistent within experimental error with the predictions of Abrikosov-Gorkov disorder-induced pair breaking [68], taking the coherence length change into account. Biaxial lattice expansion preserves tetragonal symmetry and induces Lifshitz transitions at the X and Y van Hove points simultaneously, and so may induce qualitatively different superconductivity than tuning to a single van Hove point with uniaxial pressure.

Finally, our results provide strong motivation for extending the application of piezoelectric-based strain tuning to other materials. In this work we have demonstrated that compressions up to $\sim$1% are possible, with *in situ* tunability and good strain homogeneity. The fact that we have achieved a factor of 2.3 increase of T_c of an unconventional superconductor points the way to substantial tuning of properties of other material classes as well.

Materials and Methods

Relativistic DFT electronic structure calculations were performed using the full-potential local orbital FPLO code [69–71], version fplo14.00-49. For the exchange-correlation potential, within the local density (LDA) and the the general gradient approximation (GGA) the parametrizations of Perdew-Wang [72] and Perdew-Burke-Ernzerhof [73] were chosen, respectively. The spin-orbit coupling (SOC) was treated non-perturbatively solving the four component Kohn-Sham-Dirac equation [74]. Initial calculations were performed on 8000 k-points (20×20×20 mesh), both in the LDA and GGA approximations, with and without SOC, and with and without apical oxygen relaxation. All these calculations gave similar results, with the calculated $\varepsilon_{\mathrm{vHS}}$ between -0.012 (GGA + relaxation) and -0.009 (LDA+SOC+relaxation). However proximity of the vHS to the Fermi level meant that convergence to within 3% of the calculated energy of the vHS to E_F required a higher density of k-points, so LDA+SOC+relaxation calculations were then carried out on a mesh of 343,000 k-points (70x70x70 mesh, 44766 points in the irreducible wedge of the Brillouin zone), placing $\varepsilon_{\mathrm{vHS}}$ at -0.0075.

The pressure apparatus is based on that described in Ref. [42], however there are a few key modifications that merit mention here. (1) The piezoelectric actuators were 18 mm-long Physik Instrumente PICMA® linear actuators. (2) The displacement sensor is a parallel-plate capacitor, in place of the strain gauge described in Refs. [36] and [42]. The combined strain data from four samples in this work suggest that the strains determined in Ref. [36] are ≈35% too low. One very likely contribution to this error is the mechanical resistance imposed by the strain gauge on the motion of the apparatus. Temperature shifts in the gauge coefficient of the strain gauge may also contribute. Capacitive sensors are less affected by field and temperature, and impose no mechanical resistance, so we have more confidence in the strains reported in this work. (3) The thermal contraction foils have been eliminated, allowing the core of the apparatus to be made as a single piece. The longer actuators have more than sufficient range to overcome differential thermal contraction between the sample and apparatus.

When mounting samples, a small voltage is often applied to the actuators to move the sample mount points slightly further apart. When this voltage is later released the sample is placed under modest compression. This step reduces the risk that the sample will break during cooling, for example if temperature inhomogeneity in the apparatus places the sample under inadvertent tension.

To estimate the strain applied to a sample, two pieces of information are required. The first is the origin of the strain scale, the point where the sample is under zero strain. In Ref. [36] it was determined that T_c of Sr_2RuO_4 is minimum within experimental error at zero strain, so for most samples the origin can be identified as the minimum in T_c. Two samples broke during cooling, and could be compressed by closing the crack, but not tensioned. The process of re-engaging the two ends can be gradual, *e.g.* if the two faces of the crack do not match perfectly, so zero strain cannot be reliably identified in these samples by attempting to locate the precise point where $T_c(\varepsilon_{xx})$ starts to change. Instead, a quadratic fit was made to the $T_c(\varepsilon_{xx})$ curve over a temperature range near but above the lowest observed T_c. Zero strain was identified as the minimum of the fitted curve, plus $2 \cdot 10^{-4}$ to account for the anomalous flattening of $T_c(\varepsilon_{xx})$ around $\varepsilon_{xx} = 0$ observed in Ref. [36]. The other piece of information required is an effective strained length: the capacitive sensor measures a displacement, and ε_{xx} is this displacement divided by the effective strained length. Deformation of the sample mounting epoxy means that the effective strained length is typically ∼0.4 mm longer than the exposed length of the sample. It is estimated through finite element analysis, as described in Refs. [36] and [42]. We estimate a 20% error on all strains determined in this paper.

The layers of the epoxy that secure the sample are generally 20–40 μm thick, an estimated broad optimum. Thinner layers transmit force to the sample more efficiently (*i.e.* give a shorter effective strained length), while thicker layers reduce stress concentration in the epoxy and allow greater tolerance in assembly. The dimensions, calculated effective strained length, and estimated ε_{xx} at the peak in T_c for each sample are given in Supplemental Material.

Acknowledgements

We thank Heike Pfau for experimental contributions, Eun-Ah Kim, Steven Kivelson, Srinivas Raghu, Kyle Shen and Fuchun Zhang for stimulating discussions, and Eun-Ah Kim and Fuchun Zhang for sharing the results of their calculations with us. Kim and collaborators used renormalization group calculations to study T_c versus uniaxial but mainly biaxial strain, while Liu, Zhan, Rice and Wang employed functional renormalization group calculations of the strain dependence of T_c concentrating on the d_{xy}-based Fermi surface sheet. On topics where they overlap, the reults of those two calculations, as well as the the calculations presented in this paper, are qualitatively similar. We gratefully acknowledge the support of the Max Planck Society and the UK EPSRC under grants EP/1031014/1, EP/G03673X/1, EP/N01930X/1, and EP/I032487/1. TS the support of the Clarendon Fund Scholarship, the Merton College Domus and Prize Scholarships, and the University of Oxford. Raw data for all figures in this paper are available in Supplementary Material.

* Electronic address: steppke@cpfs.mpg.de
† Electronic address: steven.simon@physics.ox.ac.uk
‡ Electronic address: mackenzie@cpfs.mpg.de
§ Electronic address: hicks@cpfs.mpg.de

[1] M. Tinkham. *Introduction to Superconductivity, 2nd edition.* ISBN-13: 978-0486435039. Dover Publications, Mineola, New York, U.S.A., 2004.
[2] A.J. Leggett. *Quantum Liquids: Bose Condensation and Cooper Pairing in Condensed-Matter Systems.* ISBN: 978-0198526438. Oxford University Press, Oxford, U.K., 2006.
[3] J.F. Annett *Superconductivity, Superfluids, And Condensates.* ISBN 0 19 850755 0. Oxford University Press, Oxford, U.K., 2005.

[4] Y. Maeno, H. Hashimoto, K. Yoshida, S. Nishizaki, T. Fujita, J.G. Bednorz, and F. Lichtenberg. Superconductivity in a layered perovskite without copper. *Nature* **372** 532 (1994).

[5] A.P. Mackenzie, R.K.W. Haselwimmer, A.W. Tyler, G.G. Lonzarich, Y. Mori, S. Nishizaki, and Y. Maeno. Extremely Strong Dependence of Superconductivity on Disorder in Sr_2RuO_4. *Phys. Rev. Lett.* **80** 161 (1998).

[6] C. Bergemann, A.P. Mackenzie, S.R. Julian, D. Forsythe, and E. Ohmichi. Quasi-two-dimensional Fermi liquid properties of the unconventional superconductor Sr_2RuO_4. *Advances in Physics* **52** 639 (2003).

[7] A. Damascelli, D.H. Lu, K.M. Shen, N.P. Armitage, F. Ronning, D.L. Feng, C. Kim, Z.-X. Shen, T. Kimura, Y. Tokura, Z.Q. Mao, and Y. Maeno. Fermi Surface, Surface States, and Surface Reconstruction in Sr_2RuO_4. *Phys. Rev. Lett.* **85** 5194 (2000).

[8] T. Oguchi. Electronic band structure of the superconductor Sr_2RuO_4. *Phys. Rev. B* **51** 1385 (1994).

[9] D.J. Singh. Relationship of Sr_2RuO_4 to the superconducting layered cuprates. *Phys. Rev. B* **52** 1358 (1995).

[10] M.W. Haverkort, I.S. Elfimov, L.H. Tjeng, G.A. Sawatzky, and A. Damascelli. Strong Spin-Orbit Coupling Effects on the Fermi Surface of Sr_2RuO_4 and Sr_2RhO_4. *Phys. Rev. Lett.* **101** 026406 (2008).

[11] T.M. Rice and M. Sigrist. Sr_2RuO_4: an electronic analogue of ^{3}He? *J. Phys: Condens. Matter* **7** L643 (1995).

[12] K. Ishida, H. Mukuda, Y. Kitaoka, K. Asayama, Z.Q. Mao, Y. Mori, and Y. Maeno. Spin-triplet superconductivity in Sr_2RuO_4 identified by ^{17}O Knight shift. *Nature* **396** 658 (1998).

[13] Ishida, K. and Manago, M. and Yamanaka, T. and Fukazawa, H. and Mao, Z. Q. and Maeno, Y. and Miyake, K. Spin polarization enhanced by spin-triplet pairing in Sr_2RuO_4probed by NMR. *Phys Rev B* **92** 100502R (2015), and references therein.

[14] M.S. Anwar, S.R. Lee, R. Ishiguro, Y. Sugimoto, Y. Tano, S.J. Kang, Y.J. Shin, S. Yonezawa, D. Manske, H. Takayanagi, T.W. Noh, and Y. Maeno. Direct penetration of spin-triplet superconductivity into a ferromagnet in $Au/SrRuO_3/Sr_2RuO_4$ junctions. Arxiv 1603.00971.

[15] G.M. Luke, Y. Fudamoto, K.M. Kojima, M.I. Larkin, J. Merrin, B. Nachumi, Y.J. Uemura, Y. Maeno, Z.Q. Mao, Y. Mori, H. Nakamura, and M. Sigrist. Time-reversal symmetry- breaking superconductivity in Sr_2RuO_4. *Nature* **394** 558 (1998).

[16] J. Xia, Y. Maeno, P.T. Beyersdorf, M.M. Fejer, and A. Kapitulnik. High Resolution Polar Kerr Effect Measurements of Sr_2RuO_4: Evidence for Broken Time-Reversal Symmetry in the Superconducting State. *Phys. Rev. Lett.* **97** 167002 (2006).

[17] S. Kashiwaya, H. Kashiwaya, H. Kambara, T. Furuta, H. Yaguchi, Y. Tanaka, and Y. Maeno. Edge States of Sr_2RuO_4 Detected by In-Plane Tunneling Spectroscopy. *Phys. Rev. Lett.* **107** 077003 (2011).

[18] F. Kidwingira, J.D. Strand, D.J. Van Harlingen, and Y. Maeno. Dynamical Superconducting Order Parameter Domains in Sr_2RuO_4. *Science* **314** 1267 (2006).

[19] K.D. Nelson, Z.Q. Mao, Y. Maeno, and Y. Liu. Odd-Parity Superconductivity in Sr_2RuO_4. *Science* **306** 1151 (2004).

[20] J.R. Kirtley, C. Kallin, C.W. Hicks, E.-A. Kim, Y. Liu, K.A. Moler, Y. Maeno, and K.D. Nelson. Upper limit on spontaneous supercurrents in Sr_2RuO_4. *Phys. Rev. B* **76** 014526 (2007).

[21] C.W. Hicks, J.R. Kirtley, T.M. Lippman, N.C. Koshnick, M.E. Huber, Y. Maeno, W.M. Yuhasz, M.B. Maple, and K.A. Moler. Limits on superconductivity-related magnetization in Sr_2RuO_4 and $PrOs_4Sb_{12}$ from scanning SQUID microscopy. *Phys. Rev. B* **81** 214501 (2010).

[22] P.J. Curran, S.J. Bending, W.M. Desoky, A.S. Gibbs, S.L. Lee, and A.P. Mackenzie. Search for spontaneous edge currents and vortex imaging in Sr_2RuO_4 mesostructures. *Phys. Rev. B* **89** 144504 (2014).

[23] S. Lederer, W. Huang, E. Taylor, S. Raghu, and C. Kallin. Suppression of spontaneous currents in Sr_2RuO_4 by surface disorder. *Phys. Rev. B* **90** 134521 (2014).

[24] A. Bouhon and M. Sigrist. Current inversion at the edges of a chiral p-wave superconductor. *Phys. Rev. B* **90** 220511R (2014).

[25] T. Scaffidi and S.H. Simon. Large Chern Number and Edge Currents in Sr_2RuO_4. *Phys. Rev. Lett.* **115** 087003 (2015).

[26] W. Huang, S. Lederer, E. Taylor, and C. Kallin. Nontopological nature of the edge current in a chiral p-wave superconductor. *Phys. Rev. B* **91** 094507 (2015).

[27] S. Yonezawa, T. Kajikawa, and Y. Maeno. First-Order Superconducting Transition of Sr_2RuO_4. *Phys. Rev. Lett.* **110** 077003 (2013).

[28] K. Deguchi, M.A. Tanatar, Z.Q. Mao, T. Ishiguro, and Y. Maeno. Superconducting Double Transition and the Upper Critical Field Limit of Sr_2RuO_4 in Parallel Magnetic Fields. *J. Phys. Soc. Japan* **71** 2839 (2002).

[29] A.P. Mackenzie and Y. Maeno. The superconductivity of Sr2RuO4 and the physics of spin-triplet pairing. *Rev. Mod. Phys.* **75** 657 (2003).

[30] Y. Maeno, S. Kittaka, T. Nomura, S. Yonezawa, and K. Ishida. *J. Phys. Soc. Japan* **81** 011009 (2012).

[31] C. Kallin. Chiral p-wave order in Sr_2RuO_4. *Rep. Prog. Phys.* **75** 042501 (2012).

[32] Y. Liu and Z.Q. Mao. Unconventional superconductivity in Sr_2RuO_4. *Physica C- Superconductivity and its Applications* **514** 339 (2015).

[33] Y. Maeno, K. Yoshida, H. Hashimoto, S. Nishizaki, S.I. Ikeda, M. Nohara, T. Fujita, A.P. Mackenzie, N.E. Hussey, J.G. Bednorz, and F. Lichtenberg. *J. Phys. Soc. Japan* **66** 1405 (1997).

[34] K.M. Shen, N. Kikugawa, C. Bergemann, L. Balicas, F. Baumberger, W. Meevasana, N.J.C. Ingle, Y. Maeno, Z.-X. Shen, and A.P. Mackenzie. Evolution of the Fermi Surface and Quasiparticle Renormalization through a van Hove Singularity in $Sr_{2-y}La_yRuO_4$. *Phys. Rev. Lett.* **99** 187001 (2007).

[35] B. Burganov, C. Adamo, A. Mulder, M. Uchida, P.D.C. King, J.W. Harter, D.E. Shai, A.S. Gibbs, A.P. Mackenzie, R. Uecker, M. Bruetzam, M.R. Beasley, C.J. Fennie, D.G. Schlom, and K.M. Shen. Strain Control of Fermiology and Many-Body Interactions in Two-Dimensional Ruthenates. *In preparation.*

[36] C.W. Hicks, D.O. Brodsky, E.A. Yelland, A.S. Gibbs, J.A.N. Bruin, M.E. Barber, S.D. Edkins, K. Nishimura, S. Yonezawa,

Y. Maeno, A.P. Mackenzie. Strong Increase of T_c of Sr_2RuO_4 Under Both Compressive and Tensile Strain. *Science* **344** 283 (2014).

[37] H. Taniguchi, K. Nishimura, S.K. Goh, S. Yonezawa, and Y. Maeno. Higher-T_c Superconducting Phase in Sr_2RuO_4 Induced by In-Plane Uniaxial Pressure.

[38] Y.A. Ying, N.E. Staley, Y. Xin, K. Sun, X. Cai, D. Fobes, T.J. Liu, Z.Q. Mao, and Y. Liu. Enhanced spin-triplet superconductivity near dislocations in Sr_2RuO_4. *Nature Comm.* **4** 2596 (2013).

[39] The elastic tensor of Sr_2RuO_4 was determined at room temperature by resonant ultrasound: J.P. Paglione, C. Lupien, W.A. MacFarlane, J.M. Perz, L. Taillefer, Z.Q. Mao, and Y. Maeno. Elastic tensor of Sr_2RuO_4. *Phys. Rev. B* **65** 220506R (2002). It gives a Young's modulus of 176 GPa, and Poisson's ratios $\nu_{xy} = 0.39$ and $\nu_{xz} = 0.21$.

[40] T. Scaffidi, J.C. Romers, and S.H. Simon. Pairing symmetry and dominant band in Sr_2RuO_4. *Phys. Rev. B* **89** 220510R (2014).

[41] O. Chmaissem, J.D. Jorgensen, H. Shaked, S. Ikeda, and Y. Maeno. Thermal expansion and compressibility of Sr_2RuO_4. *Phys. Rev. B* **57** 5067 (1998).

[42] C.W. Hicks, M.E. Barber, S.D. Edkins, D.O. Brodsky, and A.P. Mackenzie. Piezoelectric-based apparatus for strain tuning. *Rev. Sci. Inst.* **85** 065003 (2014).

[43] Stycast® 2850FT, Emerson & Cuming.

[44] L. Lyard, P. Samuely, P. Szabo, T. Klein, C. Marcenat, L. Paulius, K.H.P. Kim, C.U. Jung, H.-S. Lee, B. Kang, S. Choi, S.-I. Lee, J. Marcus, S. Blanchard, A.G.M. Jansen, U. Welp, G. Karapetrov, and W.K. Kwok. Anisotropy of the upper critical field and critical current in single crystal MgB_2. *Phys. Rev. B* **66** 180502R (2002).

[45] M. Kano, Y. Kohama, D. Graf, F. Balakirev, A.S. Sefat, M.A. McGuire, B.C. Sales, D. Mandrus, and S.W. Tozer. Anisotropy of the Upper Critical Field in a Co-Doped $BeFe_2As_2$ Single Crystal. *J. Phys. Soc. Japan* **78** 084719 (2009).

[46] T.M. Riseman, P.G. Kealey, E.M. Forgan, A.P. Mackenzie, L.M. Galvin, A.W. Tyler, S.L. Lee, C. Ager, D.McK. Paul, C.M. Aegerter, R. Cubitt, Z.Q. Mao, T. Akima, and Y. Maeno. Observation of a square flux-line lattice in the unconventional superconductor Sr_2RuO_4. *Nature* **396** 242 (1998).

[47] G. Sarma. On the influence of a uniform exchange field acting on the spins of the conduction electrons in a superconductor. *J. Phys. Chem. Solids* **24** 1029 (1963).

[48] A.M. Clogston. Upper Limit for the Critical Field in Hard Superconductors. *Phys. Rev. Lett.* **9** 266 (1962).

[49] S. Raghu, A. Kapitulnik, and S.A. Kivelson. Hidden Quasi-One-Dimensional Superconductivity in Sr_2RuO_4. *Phys. Rev. Lett.* **105** 136401 (2010).

[50] S. Nishizaki, Y. Maeno, and Z.Q. Mao. Changes in the Superconducting State of Sr_2RuO_4 under Magnetic Fields Probed by Specific Heat. *J. Phys. Soc. Japan* **69** 572 (2000).

[51] M. Sigrist, R. Joynt, and T.M. Rice. Behavior of anisotropic superconductors under uniaxial stress. *Phys. Rev. B* **36** 5186 (1987).

[52] M.H. Fischer and E. Berg. Fluctuation and strain effects in a chiral p-wave superconductor. *Phys. Rev. B* **93** 054501 (2016).

[53] H. Kusunose. Quasiclassical theory of superconducting states under magnetic fields: Thermodynamic properties. *Phys. Rev. B* **70** 054509 (2004).

[54] Y. Maeno, T. Ando, Y. Mori, E. Ohmichi, S. Ikeda, S. NishiZaki, and S. Nakatsuj. Enhancement of Superconductivity of Sr_2RuO_4 to 3 K by Embedded Metallic Microdomains. *Phys. Rev. Lett.* **81** 3765 (1998).

[55] S. Kittaka, T. Nakamura, H. Yaguchi, S. Yonezawa, and Y. Maeno. Spatial Development of Superconductivity in the Sr_2RuO_4-Ru Eutectic System. *J. Phys. Soc. Japan* **78** 064703 (2009).

[56] Y.A. Ying, Y. Xin, B.W. Clouser, E. Hao, N.E. Staley, R.J. Myers, L.F. Allard, D. Fobes, T. Liu, Z.Q. Mao, and Y. Liu. Suppression of Proximity Effect and the Enhancement of p-Wave Superconductivity in the Sr_2RuO_4-Ru System. *Phys. Rev. Lett.* **103** 247004 (2009).

[57] H. Yaguchi, M. Wada, T. Akima, Y. Maeno, and T. Ishiguro. Interface superconductivity in the eutectic Sr_2RuO_4-Ru: 3-K phase of Sr_2RuO_4. *Phys. Rev. B* **67** 214519 (2003).

[58] M. Matsumoto, C. Belardinelli, and M. Sigrist. Upper Critical Field of the 3 Kelvin Phase in Sr_2RuO_4. *J. Phys. Soc. Japan* **72** 1623 (2003).

[59] T. Nomura and K. Yamada. Roles of Electron Correlations in the Spin-Triplet Superconductivity of Sr_2RuO_4. *J. Phys. Soc. Japan* **71** 1993 (2002).

[60] Q.H. Wang, C. Platt, Y. Yang, C. Honerkamp, F.C. Zhang, W. Hanke, T.M. Rice, and R. Thomale. Theory of superconductivity in a three-orbital model of Sr_2RuO_4. *Europhysics Letters* **104** 17013 (2013).

[61] Y.-T. Hsu, W. Cho, B. Burganov, C. Adamo, A. Federico Rebola, K.M. Shen, D.G. Schlom, C.J. Fennie, and E.-A. Kim. Manipulating superconductivity in ruthenates through Fermi surface engineering. *In preparation.*

[62] Y.-C. Liu, F.-C. Zhang, T.M. Rice, and Q.-H. Wang. Theory of the Evolution of Superconductivity in Sr_2RuO_4 under Uniaxial Strain. *In preparation.*

[63] I. Žutić and I. Mazin. Phase-Sensitive Tests of the Pairing State Symmetry in Sr_2RuO_4. *Phys. Rev. Lett.* **95** 217004 (2005).

[64] R. Jin, Yu. Zadorozhny, Y. Liu, D.G. Schlom, Y. Mori, and Y. Maeno. Observation of anomalous temperature dependence of the critical current in $Pb/Sr_2RuO_4/Pb$ junctions. *Phys. Rev. Lett.* **59** 4433 (1999).

[65] T. Nakamura, R. Nakagawa, T. Yamagishi, T. Terashima, S. Yonezawa, M. Sigrist, and Y. Maeno. Topological competition of superconductivity in $Pb/Ru/Sr_2RuO_4$ junctions. *Phys. Rev. B* **84** 060512R (2011).

[66] M.S. Anwar, T. Nakamura, S. Yonezawa, M. Yakabe, R. Ishiguro, H. Takayanagi, and Y. Maeno. Anomalous switching in $Nb/Ru/Sr_2RuO_4$ topological junctions by chiral domain wall motion. *Sci. Reports* **3** 2480 (2013).

[67] H. Kambara, S. Kashiwaya, H. Yaguchi, Y. Asano, Y. Tanaka, and Y. Maeno. Anomalous Transport through the p-Wave Superconducting Channel in the 3-K Phase of Sr_2RuO_4. *Phys. Rev. Lett.* **101** 267003 (2008).

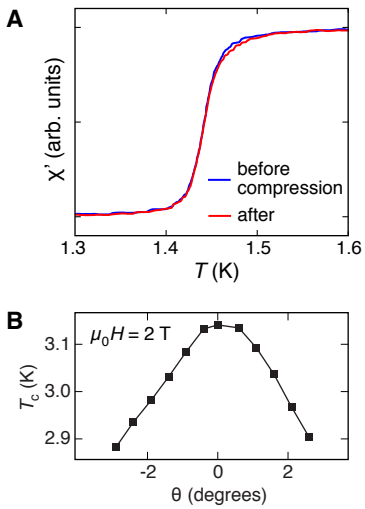

FIG. 9: **Additional data. A.** $\chi'(T)$ of sample 1 at zero strain, before and after compression to the T_c peak. **B.** T_c against field angle θ for sample 4, at a constant field $\mu_0 H = 2$ T. θ is in the **a**-**c** plane, and $\theta = 0$ corresponds to $\mathbf{H} \parallel \mathbf{a}$.

[68] A. A. Abrikosov and L. P. GorâĂŹkov, *Zh. Eksp. Teor. Fiz.* **39** 1781 (1960) [*Sov. Phys. JETP* **12** 1243 (1961)].
[69] K. Koepernik and H. Eschrig. Full-potential nonorthogonal local-orbital minimum-basis band-structure scheme. *Phys. Rev. B* **59** 1743 (1999).
[70] I. Ophale, K. Koepernik, and H. Eschrig. Full-potential band-structure calculation of iron pyrite. *Phys. Rev. B* **60** 14035 (1999).
[71] http://www.fplo.de
[72] J.P. Perdew and Y. Wang. Accurate and simple analytic representation of the electron-gas correlation energy. *Phys. Rev. B* **45** 13244 (1992).
[73] J.P. Perdew, K. Burke, and M. Ernzerhof. Generalized Gradient Approximation Made Simple. *Phys. Rev. Lett.* **77** 3865 (1996).
[74] H. Eschrig, M. Richter, and I. Opahle. Relativistic Solid State Calculations, in: *Relativistic Electronic Structure Theory, (Part II, Applications)* (ed. P. Schwerdtfeger), *Theoretical and Computational Chemistry*, vol.13, Elsevier, 723, (2004)
[75] E. Ohmichi, Y. Maeno, S. Nagai, Z.Q. Mao, M.A. Tanatar, T. Ishiguro. Magnetoresistance of Sr_2RuO_4 under high magnetic fields parallel to the conducting plane. *Phys. Rev. B* **61** 7101 (2000).
[76] M.E. Zhitomirsky and T.M. Rice. Interband Proximity Effect and Nodes of Superconducting Gap in Sr_2RuO_4. *Phys. Rev. Lett.* **87** 057001 (2001).

Supplemental Material

Additional data. Some supplementary data are shown in Fig. 9. Panel A shows $\chi'(T)$ of sample #1 before and after it was pressurized to $T_c = 3.4$ K. There is evidence that applying high uniaxial pressure at room temperature can introduce dislocations [37], which in turn can induce local higher-T_c superconductivity [38]. However here almost no change is observed after compression. For all samples studied here, data was taken with both increasing and decreasing strains, with no obvious change in the observed $\chi'(T)$ curves.

Panel B shows T_c against field angle for fields close to the plane, at a constant field magnitude of 2 T, and confirms a sharp dependence on field angle for fields close to the ab plane. In another check of whether the H_{c2} data presented in Fig. 5 are really at the peak, H_{c2} at 1.6 K was measured while the compression on this sample was varied slightly around the peak. In this check $H_{c2\|a}(\varepsilon_{xx})$ was found to be rounded at the peak, like T_c, and $\mu_0 H_{c2\|a}(1.6\text{ K})$ in Fig. 5 is within 0.02 T of the peak.

Sample dimensions are given in Table 1. In the table, w and t are the sample width and thickness, $l_{\rm exp}$ is the exposed length of the sample, and $t_{\rm epoxy}$ is the epoxy thickness. $l_{\rm eff}$ is the effective strained length of the sample, where the sample strain is given by the displacement measured by the displacement sensor divided by $l_{\rm eff}$. $l_{\rm eff}$ is longer than $l_{\rm exp}$ because the strain field extends into the sample mounts, and is calculated by finite element analysis. $\varepsilon_{\rm peak}$ is ε_{xx} at the peak in T_c, determined independently for each sample. The observed sample-to-sample variation almost certainly reflects experimental uncertainty in determining $\varepsilon_{\rm peak}$ rather than intrinsic sample-to-sample variation. $\varepsilon_{\rm peak}$ is not

TABLE I: **Sample dimensions.** Relevant parameters for calculating the sample strain, explained in the text.

number	w (μm)	t (μm)	$l_{\rm exp}$ (μm)	$t_{\rm epoxy}$ (μm)	$l_{\rm eff}$ (μm)	$\varepsilon_{\rm peak}$ (10^{-2})
1	≈250	≈50	660	≈10	830	-0.66
2	241	44	1620	≈20	2020	-0.63
3	295	100	1000	≈25	1430	-0.51
4	234	96	1460	–	–	
5	310	100	1000	≈25	1430	-0.59

reported for sample 4 because repeated rupturing of the epoxy meant that $l_{\rm eff}$ could not be determined with confidence.

Details of the RG calculation, and results at $J/U = 0.08$. The strain-dependent hopping Hamiltonian $H_0(\epsilon)$ is

$$H_0(\varepsilon) = \sum_{\mathbf{k},s} \psi_s^\dagger(\mathbf{k}) \hat{H}_s(\varepsilon, \mathbf{k}) \psi_s(\mathbf{k}),$$

where $\psi_s(\mathbf{k}) = \left[c_{\mathbf{k},A,s} c_{\mathbf{k},B,s} c_{\mathbf{k},C,-s}\right]^T$. ε is taken to mean the longitudinal strain, ε_{xx}. A, B, and C respectively indicate the Ru $4d_{xz}$, $4d_{yz}$, and $4d_{xy}$ orbitals on each lattice site, and $s = 1$ (-1) for up (down) spins. The matrix $\hat{H}_s(\varepsilon, \mathbf{k})$ is given by

$$\hat{H}_s(\varepsilon, \mathbf{k}) = \begin{pmatrix} E_A(\varepsilon, \mathbf{k}) & g(\mathbf{k}) - si\eta & i\eta \\ g(\mathbf{k}) + si\eta & E_B(\varepsilon, \mathbf{k}) & -s\eta \\ -i\eta & -s\eta & E_C(\varepsilon, \mathbf{k}) \end{pmatrix},$$

where

$$\begin{aligned} E_A(\varepsilon, \mathbf{k}) &= -2t_x(\varepsilon)\cos(k_x) - 2t_y^\perp(\varepsilon)\cos(k_y) - \mu(\varepsilon), \\ E_B(\varepsilon, \mathbf{k}) &= -2t_y(\varepsilon)\cos(k_y) - 2t_x^\perp(\varepsilon)\cos(k_x) - \mu(\varepsilon), \\ E_C(\varepsilon, \mathbf{k}) &= -2t_x'(\varepsilon)\cos(k_x) - 2t_y'(\varepsilon)\cos(k_y) - 4t''\cos(k_x)\cos(k_y) - \mu_C(\varepsilon), \\ g(\mathbf{k}) &= -4t'''\sin(k_x)\sin(k_y). \end{aligned}$$

η is the spin-orbit coupling parameter and $g(\mathbf{k})$ is the inter-orbital hopping term. The strain-dependent hoppings are given by

$$\begin{aligned} t_x(\varepsilon) &= t(1 - a\varepsilon), \\ t_y(\varepsilon) &= t(1 + a\nu_{xy}\varepsilon), \\ t_x^\perp(\varepsilon) &= t^\perp(1 - a\varepsilon), \\ t_y^\perp(\varepsilon) &= t^\perp(1 + a\nu_{xy}\varepsilon), \\ t_x'(\varepsilon) &= t'(1 - a\varepsilon), \\ t_y'(\varepsilon) &= t'(1 + a\nu_{xy}\varepsilon), \end{aligned}$$

where, as noted in the main text, ν_{xy} is the in-plane Poisson's ratio [39], and a is an adjustable parameter that places the Lifshitz transition at $\varepsilon_{xx} = -0.0075$, as determined in the DFT calculation. The zero-strain parameters are chosen to fit the experimental Fermi surfaces, as described in Ref. [40]; in dimensionless units, $(t, t^\perp, t', t'', \mu, \mu_C, t''', \eta) = (1.0, 0.1, 0.8, 0.3, 1.0, 1.1, 0.01, 0.1)$. The chemical potentials μ and μ_C are adjusted with strain to $\mu + \delta\mu(\varepsilon)$ and $\mu_C + \delta\mu_C(\varepsilon)$ so that the filling of each orbital remains constant at ≈4/3.

The critical field at zero temperature $H_{c2\|c}(T \to 0)$ is calculated in the quasi-classical limit, following Ref. [53]. It is given by

$$H_{c2} = 2\pi e^{-\gamma} \frac{\Phi_0}{\hbar^2} T_c^2 \exp\left[-2\left\langle |\psi_\mu(\mathbf{k})|^2 \log(\tilde{v}_\mu(\mathbf{k}))\right\rangle\right],$$

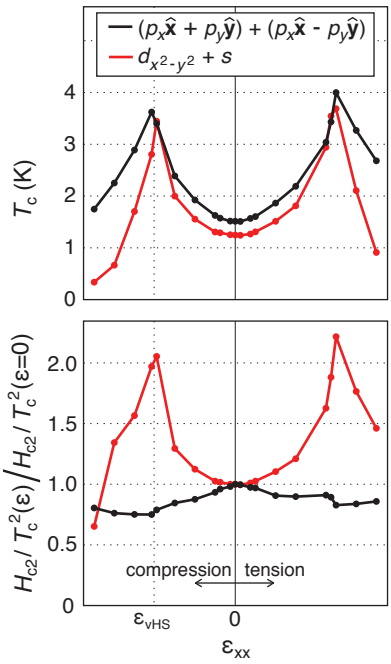

FIG. 10: ***J/U*=0.08 RG calculation results.** Upper panel: T_c against strain of the odd-parity, helical order $p_x\hat{\mathbf{x}} + p_y\hat{\mathbf{y}}$ and the even-parity order $d_{x^2-y^2}$ with $J/U = 0.08$. The bandwidth and U/t have been set, independently of the $J/U = 0.06$ calculations presented in the main text, to place the highest zero-strain T_c at 1.5 K, and the peaks at ∼3.4 K. When $\varepsilon_{xx} \neq 0$, $d_{x^2-y^2}$ becomes $d_{x^2-y^2} + s$, and $p_x\hat{\mathbf{x}} + p_y\hat{\mathbf{y}}$ becomes $(p_x\hat{\mathbf{x}} + p_y\hat{\mathbf{y}}) + (p_x\hat{\mathbf{x}} - p_y\hat{\mathbf{y}})$. Lower panel: dependence of $H_{c2\|c}/T_c^2$ on strain.

where μ is the band index, $\gamma \approx 0.577216$ is Euler's constant, and Φ_0 is the flux quantum. $\psi(\mathbf{k})$ is an eigenvector of the RG matrix; $\Delta(\mathbf{k}) \propto \psi(\mathbf{k})$. $\langle ... \rangle$ is the Fermi surface average, $\langle ... \rangle = \sum_\mu S_{F,\mu}^{-1} \int_{S_{F,\mu}} d\mathbf{k}$....

$$\tilde{v}_\mu(\mathbf{k}) = \sqrt{\chi^{-1/2} v_{x,\mu}(\mathbf{k})^2 + \chi^{1/2} v_{y,\mu}(\mathbf{k})^2},$$

where $\chi = \overline{v_{x,\mu}^2}/\overline{v_{y,\mu}^2}$ with $\overline{v_{x,u}^2} = \rho_\mu^{-1} \int_{S_{F,\mu}} d\mathbf{k} v^{-1} v_x^2$, where v_x is the x component of the Fermi velocity. For c-axis critical fields, the direction subscripts x and y indicate the (100) and (010) lattice directions.

$J/U = 0.06$ results are shown in the main text. We show $J/U = 0.08$ results here. The strain evolution of T_c and $H_{c2\|c}/T_c^2$ is shown in Fig. 10. They are very similar to the $J/U = 0.06$ results. One difference is that because the gap of the odd-parity order is initially larger on the α and β sheets, rather than on γ as with $J/U = 0.06$, the suppression of $H_{c2\|c}/T_c^2$ with tuning to the van Hove singularity is not as strong. Another noteworthy feature is that the orientation of the d-vector, shown in the upper panels, has a very similar structure to that of the phase of the odd-parity $J/U = 0.06$ results.

2D versus 3D. Sr_2RuO_4 is a highly two-dimensional material, with $\rho_c/\rho_{ab} \approx 4000$ at 2 K [75]. The discussion in the paper is easiest to understand in a fully two-dimensional picture, in which the first Brillouin zone is that of an isolated RuO_2 sheet, *i.e.* it is a square. In this picture, uniaxial pressure induces elliptical distortion of the γ Fermi surface that eventually pushes it through a Lifshitz transition at a single van Hove point that by symmetry is located on the 2D zone boundary. This point is invariant under parity inversion, so odd-parity order parameters must have zero amplitude at this point.

Although we expect that this is a qualitatively accurate description of Sr_2RuO_4, the three-dimensional behavior is slightly more complicated. The 3D first Brillouin zone is shown in Fig. 12A. The Lifshitz transition occurs along lines that run mostly vertically and do not coincide with the zone boundary. In the presence of 3D interplane coupling, it will not occur at the same strain at every point along the line, although the highly 2D nature of Sr_2RuO_4 means that the transition likely spans only a narrow range of ε_{xx}. Two points on this line are highlighted in the figure by a solid and an open point, and for illustration the equivalent points in adjacent zones are also shown. The two points are

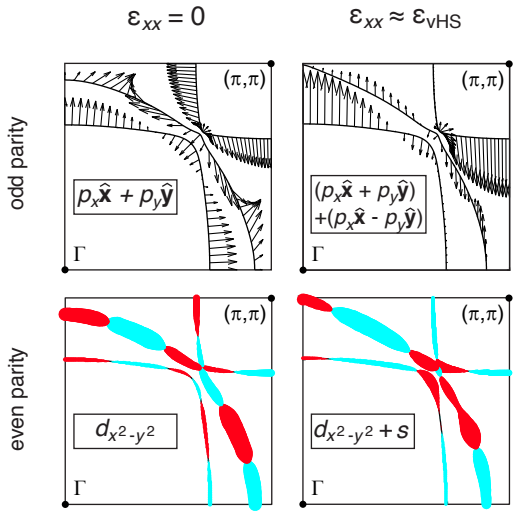

FIG. 11: ***J/U*=0.08 order parameters.** The arrows in the upper panels are the d-vectors of the helical $\mathbf{d} \sim p_x\hat{\mathbf{x}} + p_y\hat{\mathbf{y}}$ ($\varepsilon_{xx} = 0$) and $(p_x\hat{\mathbf{x}} + p_y\hat{\mathbf{y}}) + (p_x\hat{\mathbf{x}} - p_y\hat{\mathbf{y}})$ ($\varepsilon_{xx} \neq 0$) irreducible representations.

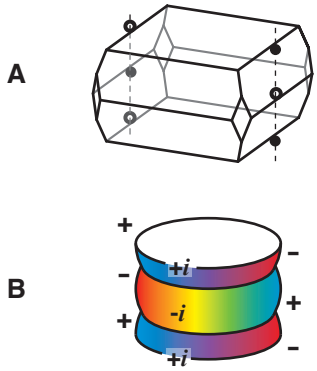

FIG. 12: **Complications in three dimensions. A.** The 3D first Brillouin zone of Sr_2RuO_4. The Lifshitz transition occurs along the vertical dashed lines. Two points, the solid and open points, are highlighted for illustration; in 2D they are equivalent points, but in the 3D zone of Sr_2RuO_4 they are not. **B.** Chiral order with horizontal line nodes, which would not be frustrated at the Lifshitz transition.

equivalent in two dimensions but not, in principle, in three dimensions. In principle, this means that the frustration of odd-parity order could be relieved with horizontal line nodes; the energy gap of $p_x \pm ip_y$ order, for example, would have the form $\Delta \sim (\sin(k_x/2)\cos(k_y/2) + i\sin(k_y/2)\cos(k_x/2))\cos(k_z/2)$, as illustrated in panel B. In Ref. [76], it was proposed that interband scattering could yield precisely such horizontal nodes on the passive bands alone. However such nodes on the active band seem generally unlikely, because they would require strong interplane pairing and hence strong interplane coupling, and furthermore such an odd-parity order parameter would not explain the appearance of a Pauli-limited $H_{c2\|a}$.